



---

**Impact of Quadrupole offset and  
Undulator end-kicks on the  
European-XFEL facility Performance**

Yuhui Li, Bart Faatz and Joachim Pflueger

*Deutsches Elektronen Synchrotron (DESY), Hamburg,  
Germany*



May 2009, TESLA-FEL 2009-04

---



# Impact of Quadrupole offset and Undulator end-kicks on the European-XFEL facility Performance

Yuhui Li, Bart Faatz and Joachim Pflueger

*Deutsches Elektronen-Synchrotron (DESY), Hamburg, Germany*

## Abstract

The undulator system for European-XFEL is longer than 100 m. To constrain the electron beam size over such a long distance, quadrupoles are necessary between undulator segments. Misaligned quadrupoles kick the electron beam and thus generate beam wander as well as phase shake, both of which reduce the FEL performance. At both ends of each undulator segment, the electron beam is also kicked due to gap dependent end fields with a similar impact. In this report, the effect of both is investigated. An upper limit of quad-offset and end-kick is given.

**Key words:** tolerance, undulator, XFEL, quadrupole offset, end-kick

## 1 Introduction

The European-XFEL facility will supply high brilliance of X-ray radiation for a large variety of experiments [1]. It uses the so-called Self-Amplified Spontaneous Emission (SASE) configuration [2, 3]. Three undulator lines named SASE1, SASE2 and SASE3 will be constructed. SASE1 will supply radiation down to 0.1 nm with a fixed gap undulator, SASE2 will generate 0.1 to 0.4 nm X-ray by gap variation for the same energy and SASE3 will deliver radiation at longer wavelengths between 0.4 and 1.6 nm.

Because the gain length is long at these short wavelengths, the undulator system is longer than 100 m [4]. For such a long undulator system, the undulator must be divided into many segments and quadrupoles are necessary to focus the electron beam. Quadrupole misalignment is unavoidable and unfortunately the quadrupole offset kicks the electron beam. A similar effect occurs when the electron passes the entrance and exit of each undulator segment. The induced transverse movement of the electron reduces the overlap of electron beam and optical field as well as break their synchronous relationship. Both can degrade the performance. Earlier studies show that the power reduction is well correlated with beam wander and phase shake [5, 6, 7, 8]. Therefore, in this report we study the quadrupole offset and undulator end-kick due to beam wander. Impact of phase shake is also discussed.

Because the tolerances are expected to be most stringent for the shorter wavelengths, the results are analyzed for SASE1 and SASE2. The 3D simulation code Genesis 1.3 which can include undulator as well as quadrupole errors is used for the simulation [9].

## 2 Description of quadrupole offset and undulator end-kick

If a quadrupole has an offset with respect to the electron beam, the beam will be kicked. Assuming  $x$  and  $y$  are quadrupole offset in the transverse direction relative to the beam and  $g$  is the gradient of quadrupoles (in T/m), the magnet field is:

$$B_y = -g \cdot x, B_x = -g \cdot y. \quad (1)$$

The transverse momentum change  $dP_x$  and  $dP_y$  is:

$$dP_x = -e \cdot g \cdot x L_{quad}, dP_y = -e \cdot g \cdot y L_{quad}, \quad (2)$$

where  $L_{quad}$  is the length of quadrupole and  $e$  is the electron charge.

For illustration, Fig. 1 shows the kick angle (a), beam wander (b) and phase (c) due to random quad-offset in the  $x$ -direction along the undulator. It can be seen that  $x'$  in each undulator segment varies randomly. Therefore, the electron beam center  $\langle x \rangle$  along the undulator and the ponderomotive phase  $\phi$  vary accordingly.

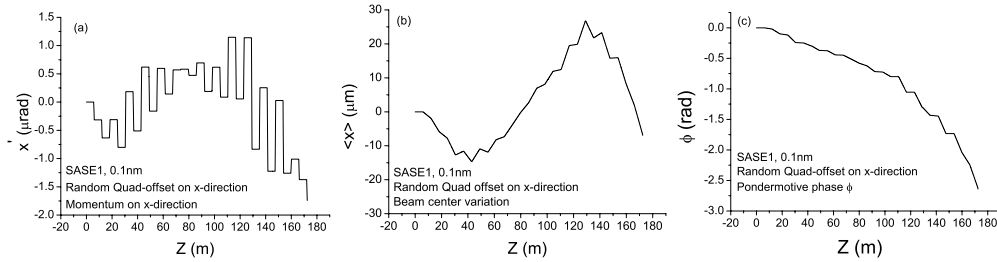


Figure 1: *Impact of random quadrupole offset in  $x$ -direction. Shown are the kick angle (a), beam orbit (b) and phase (c) of the electron beam along the undulator.*

Kicks at undulator entrance and exit have similar impact on the electron beam as a quadrupole offset. There are two types of undulator end-kicks. One is that kick at entrance and exit have the same amplitude and sign: to this kick we refer as unidirectional, as illustrated in Fig. 2. The other is that the kick at the undulator entrance and exit have the same amplitude but opposite sign (see Fig. 3).

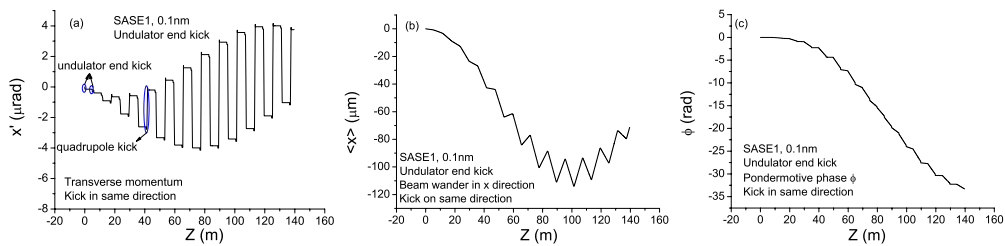


Figure 2: *Undulator end-kick, both entrance and exit kicks are in the same direction. Shown are the angle in  $x$ -direction (a), the corresponding beam orbit (b) and phase (c) of the electron beam along the undulator.*

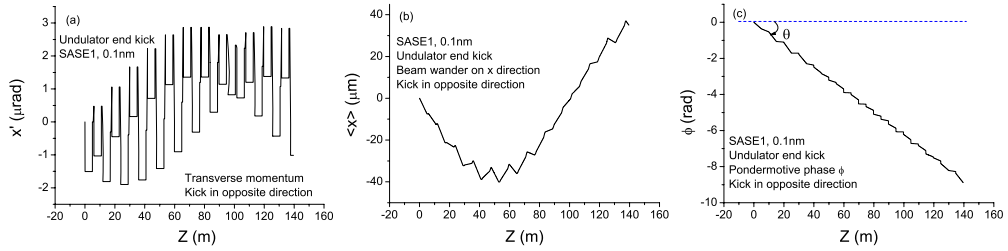


Figure 3: *Undulator end-kick with entrance and exit kicks in opposite direction. Shown are the angle in  $x$ -direction (a), the corresponding beam orbit (b) and phase (c) of the electron beam along the undulator.*

Fig. 2 shows the impact of the unidirectional end-kick. From (a) it can be seen that at all of the undulator ends,  $x'$  is continuously kicked to negative values. After several undulator segments,  $|x'|$  accumulates to a large value of  $x$  until the kicks by quadrupoles become the dominant effect, kicking the beam back to the undulator axis as shown in Fig. 2b. Fig. 3 shows the impact of opposite direction end-kick. Plot (a) clearly illustrates that the  $x'$ -variation due to the entrance kick is compensated by the exit kick. Compared to Fig. 2, a larger end-kick results in the same beam wander amplitude. From plot (c) the slope of the ponderomotive phase variation is constant, which results in an angle  $\theta$  corresponding to a wavelength shift as we will show in appendix B. However, since the wavelength shift is small in all relevant cases, it will be neglected for the (random) quadrupole offset and only be checked for the undulator end-kicks.

In Fig. 2b, one can see that the beam wanders predominantly in one direction. As a consequence, the radiation is emitted in the same direction and the power reduction may in fact be minimal. Therefore, in the remainder of this report, when we discuss beam wander, we refer to a deviation from a straight line which does not necessarily coincide with the undulator axis. Some details can be found in Appendix C.

As can also be seen in all previous figures is that due to a phase changed, the wavelength is shifted and a phase shake is added on top of the beam wander. Because the phase shake is caused by a transverse velocity component, there is a one-to-one relation beam wander and phase shake. Because we focus in this paper on the effect of beam wander and do not always include the phase shake, the power reduction for different undulator and electron beam parameters may be different. Some remarks on the relation between beam wander and phase shake can be found in Appendix D.

### 3 Simulation result for quadrupole offset

#### 3.1 result of SASE1

For the quadrupole offset simulation, we randomly change the transverse position in the range of  $[-\delta, +\delta]$  for every quadrupole. The threshold  $\delta$  is set as 1, 2, 5  $\mu\text{m}$  and for each  $\delta$ , 100 random simulations are done.

From the European XFEL project design report, the  $\beta$ -function is 32 m and the length of one undulator segment is 5 m, the intersection length is around 1 m. Normally a quadrupole is set in each intersection, so the FODO period is around 12 m. However, since for this value of  $\beta$ , one can have a FODO period of 24 m, which means one quadrupole is set for every two intersections. Therefore, also this option is studied.

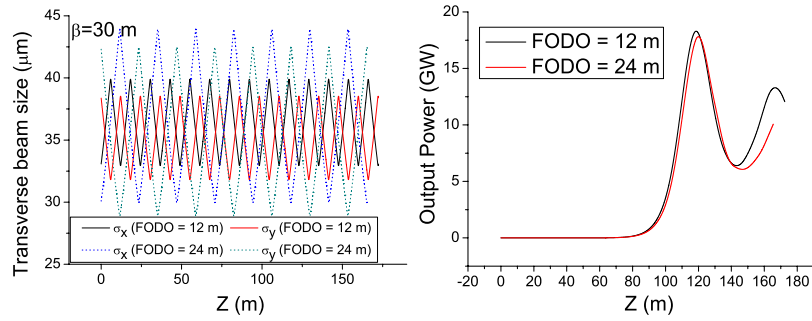


Figure 4: Transverse beam size (left) and power growth (right) for difference FODO periods along the undulator. Both plots illustrate the result without Quadrupole offset.

Fig. 4 shows the electron beam size and power growth for the two different FODO periods. The left plot shows that for both FODO periods the average transverse beam size is about  $35\ \mu\text{m}$ , although the longer FODO period has larger beam size variation. From the right plot it can be seen that there is no significant difference in the power growth for the two different FODO period.

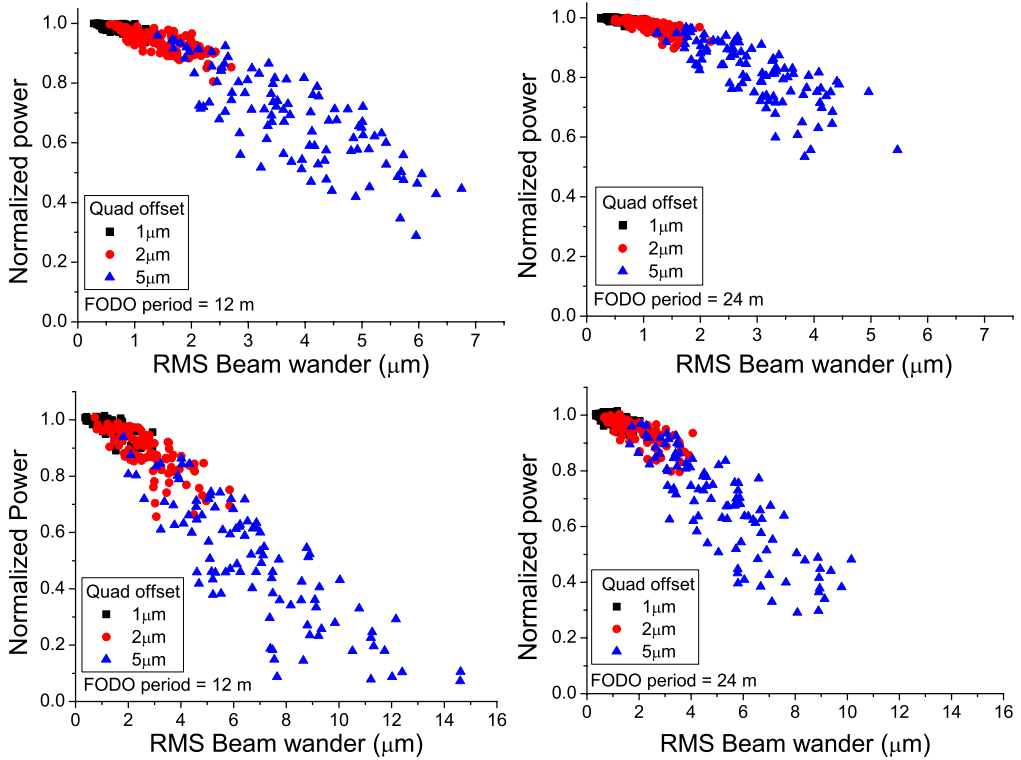


Figure 5: Power degradation versus RMS beam wander, the power is taken from the point of 70% (top, corresponding to the exponential gain regime) and 90% (bottom, corresponding to a point close to saturation) saturation length. Left: FODO period = 12 m, Right: FODO period = 24 m.

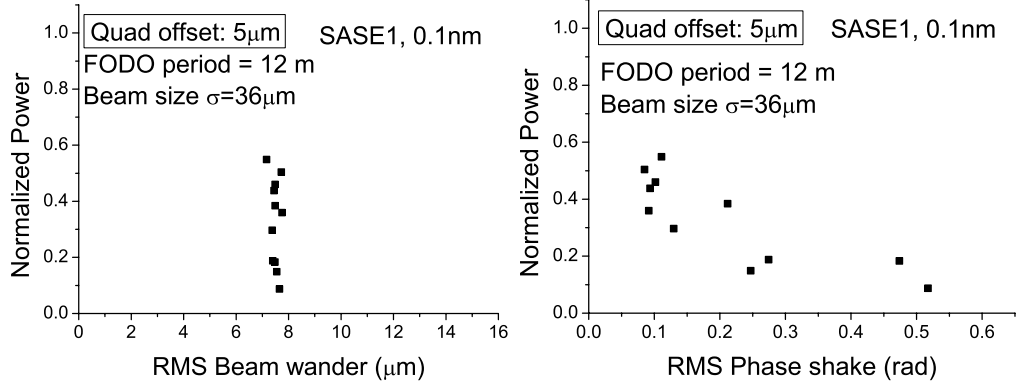


Figure 6: Comparison of power degradation variation as RMS beam wander and RMS phase shake. From the left plot the RMS beam wander is same, while the power spread is large. From the right plot the power degrades as RMS phase shake, this explains in some extent why same beam wander has large power spread. the power is taken from the point of 95% saturation length. FODO=12 m

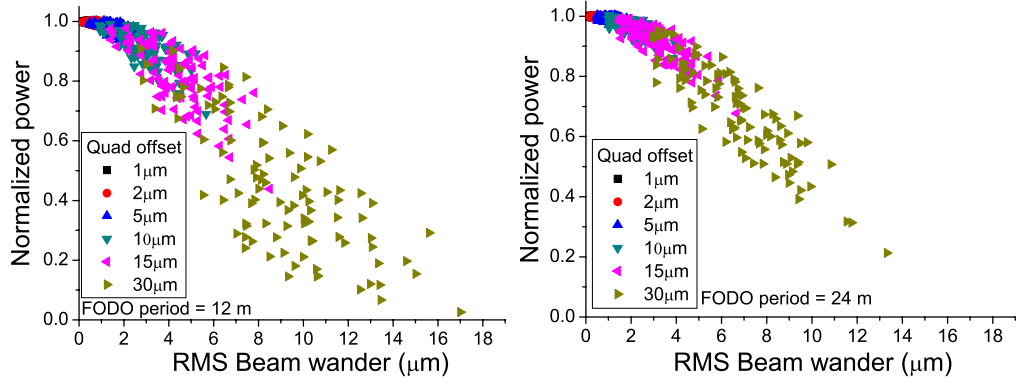


Figure 7: Power degradation at different RMS beam wander for SASE1, 0.4 nm, the power is taken from the point of 70% saturation length. Left: FODO period = 12 m, Right: FODO period = 24 m.

Fig. 5 shows the simulation result for SASE1, 0.1 nm. The position at which power is evaluated is 70% of the saturation length, which is in the exponential gain regime, and 95%, which is close to saturation. The left plots show the case of FODO period is 12 m and the right plots show the FODO period equal to 24 m. One can see that for both FODO period simulation, when the quadrupole offset is smaller than 2  $\mu\text{m}$ , the RMS beam wander is smaller than 3  $\mu\text{m}$  and the power is larger than 80%. If the quadrupole offset is increased to 5  $\mu\text{m}$ , the largest RMS beam wander extends to around 6  $\mu\text{m}$  and the power degradation becomes too large.

For a given RMS beam wander, the variation in power is increasingly large for quadrupole offsets exceeding 5  $\mu\text{m}$ . the reason for this could be a difference in RMS phase shake. In Fig. 6 some simulation points in Fig.5 which have similar RMS beam wander are shown. From the plot on the right in Fig. 6 it can be seen that the power degrades due to an increase in RMS phase shake.

An important conclusion that can be drawn from the simulations is that a given quadrupole offset results in a smaller beam wander and therefore a smaller power reduction in case of the longer FODO period. Based on this the SASE1 simulations clearly favor a 24 m FODO period.

### 3.2 Result for SASE2

In this section, the quadrupole offset simulation results for SASE2 is illustrated. The simulation method is same to the SASE1, so in this section we only list the result.

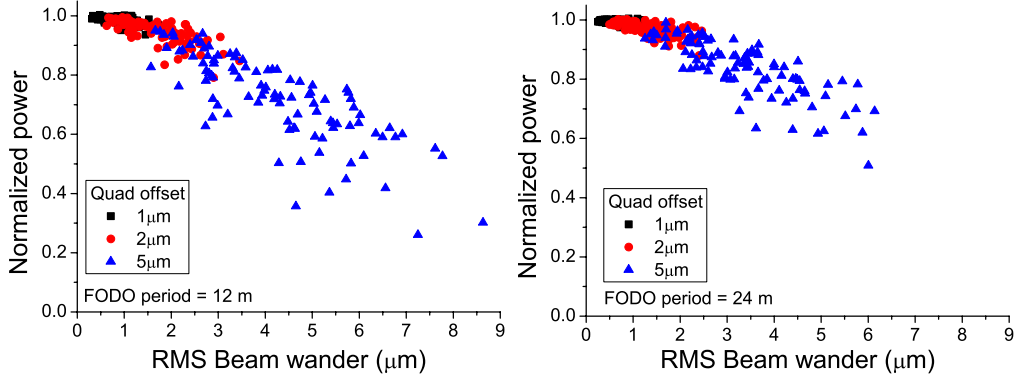


Figure 8: Power degradation at different RMS beam wander for SASE2, 0.1 nm, the power is taken from the point of 70% saturation length. Left: FODO period = 12 m, Right: FODO period = 24 m.

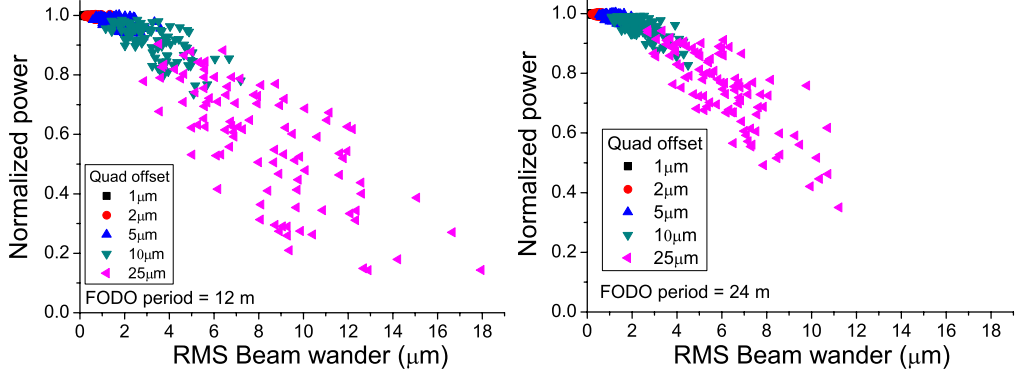


Figure 9: Power degradation at different RMS beam wander for SASE2, 0.4 nm, changing electron energy,  $\beta = 45$  m, the power is taken from the point of 70% saturation length. Left: FODO period = 12 m, Right: FODO period = 24 m.

### 3.3 Power degradation scaled by the value of RMS beam wander over beam size ( $\sigma_r/\sigma_b$ )

It is interesting to compare the power degradation among the SASE1, SASE2 different modes. In this report the power degradation is mainly scaled by RMS beam wander.

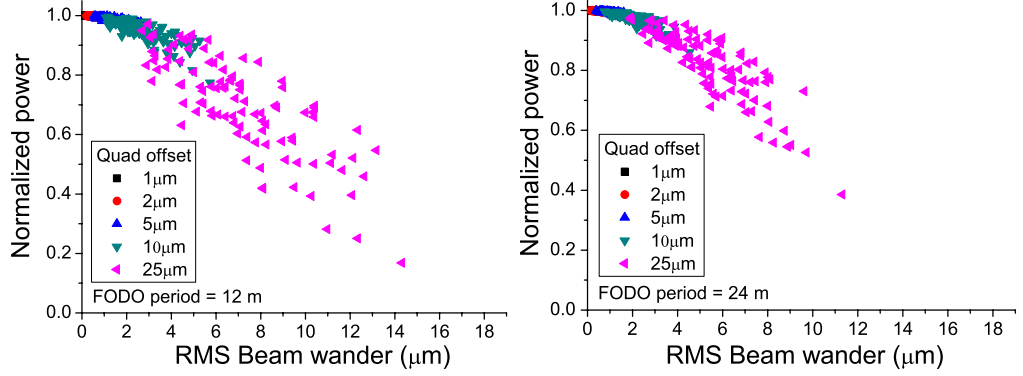


Figure 10: Power degradation at different RMS beam wander for SASE2, 0.4 nm, changing undulator gap,  $\beta = 45$  m, the power is taken from the point of 70% saturation length. Left: FODO period = 12 m, Right: FODO period = 24 m.

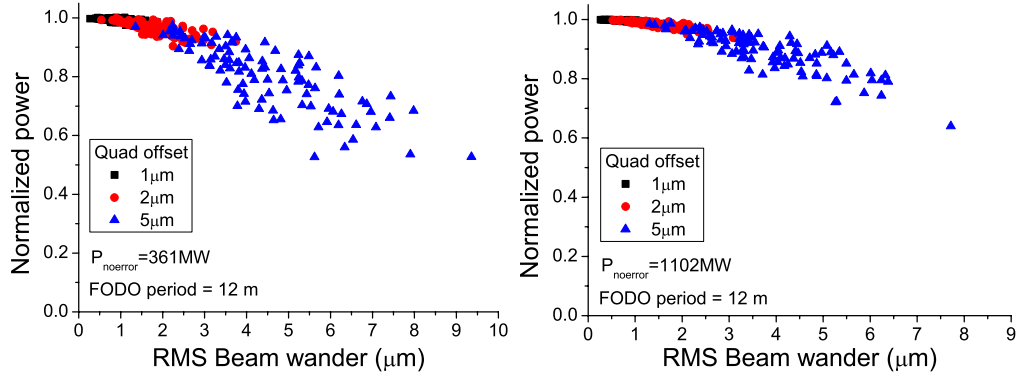


Figure 11: Power degradation at different RMS beam wander for SASE2, 0.4 nm, changing electron beam energy (left) or undulator gap (right),  $\beta = 15$  m, the power is taken from the point of 70% saturation length for a FODO period = 12 m. The small  $\beta$ -function cannot be achieved with a FODO period of 24 m.

Because in different operation modes electron beam size has different value, in Fig. 12 the RMS beam wander is normalized to the electron beam size ( $\sigma_r/\sigma_b$ ).

Fig. 12 includes four different SASE modes: SASE1, 0.1 nm; SASE1, 0.4 nm by changing the electron energy; SASE2, 0.1 nm and SASE2, 0.4 nm by changing the electron energy. One can see that the power degradation roughly overlap each other. But we should careful to do this kind of comparison, because RMS phase shake also plays a role in reducing radiation power in this case and it is not included in the illustration.

## 4 Result for undulator end-kick for SASE1 and SASE2

Fig. 13 shows the power degradation by undulator end-kick. From the left plot one can see that kicking on opposite direction permits larger kick angle. This is because the kick direction at the entrance and exit is opposite, when the electron beam enters an undulator segment it gets a transverse momentum, while when it passes the exit

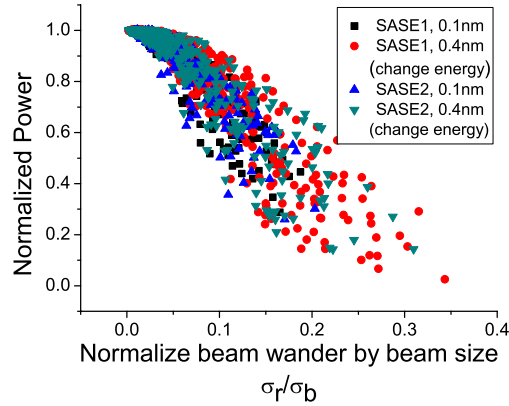


Figure 12: Power degradation scaled by the value of RMS beam wander over beam size. the power is taken from the point of 70% saturation length; FODO period = 12 m.

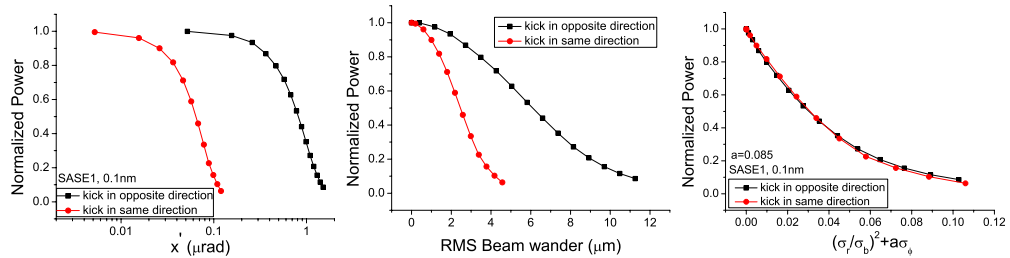


Figure 13: Power degradation by undulator end-kick for SASE1 at 0.1 nm versus initial kick angle (Left), beam wander (Middle) and a combination of the square of beam wander and phase shake (Right).

undulator, the momentum is corrected.

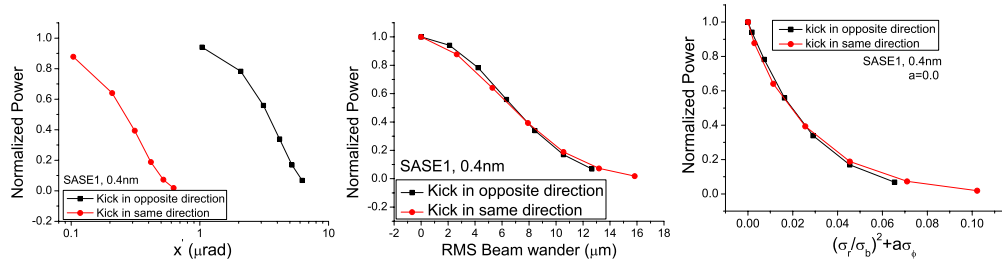


Figure 14: Power degradation by undulator end-kick for SASE1 at 0.4 nm versus initial kick angle (Left), beam wander (Middle) and a combination of the square of beam wander and phase shake (Right).

From the middle plot one can see that if the RMS beam wander is the same, a kick in opposite direction has larger power. This is because the RMS phase shake is smaller for it (see to Fig. 24). Because both phase shake and beam wander can degrade radiation power we combine the RMS beam wander  $\sigma_r$  and the RMS phase shake  $\sigma_\phi$  together

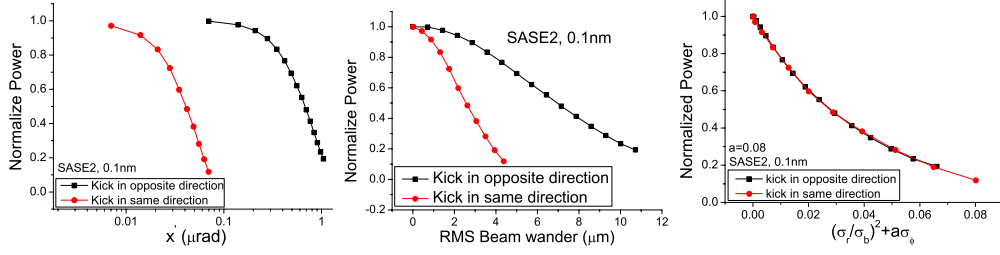


Figure 15: Power degradation by undulator end-kick for SASE2, 0.1 nm versus initial kick angle (Left), beam wander (Middle) and a combination of the square of beam wander and phase shake (Right).

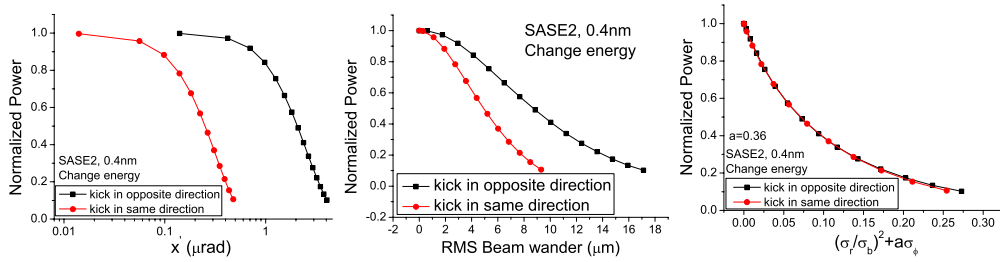


Figure 16: Power degradation by undulator end-kick for SASE2 at 0.4 nm by changing the beam energy versus initial kick angle (Left), beam wander (Middle) and a combination of the square of beam wander and phase shake (Right).

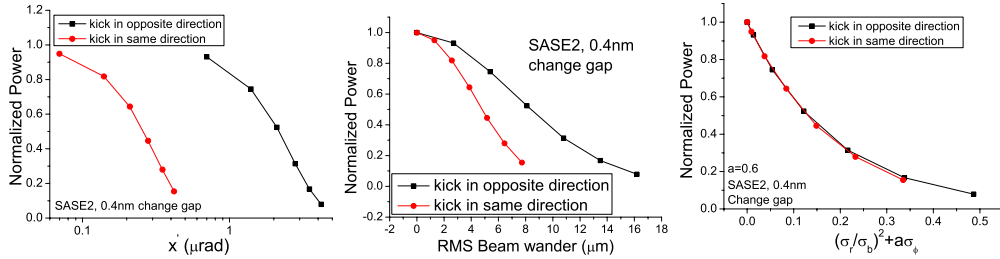


Figure 17: Power degradation by undulator end-kick for SASE2, 0.4 nm by changing undulator gap versus initial kick angle (Left), beam wander (Middle) and a combination of the square of beam wander and phase shake (Right).

into a new number to scale power degradation. As analyzed in the Appendix D,  $\sigma_r^2$  is proportional to  $\sigma_\phi$ , so the new number can be defined as:

$$(\sigma_r/\sigma_b)^2 + a \cdot \sigma_\phi$$

where  $a$  is a parameter to be determined that makes the curves of opposite direction end-kick and same direction end-kick overlap. This scaling is shown in the plots on the right. As can be seen, both for SASE1 and SASE2 at 0.1 nm, the contribution of phase shake to the power degradation is moderate and has a similar magnitude. For 0.4 nm, there is no clear tendency. For SASE1, phase shake seems to play no role what-so-ever.

For SASE2, the influence of phase shake is more pronounced and the dependence on gap or energy variation seems different. This issue deserves further study, but has not been studied further in this report.

## 5 Summary and conclusion

The simulations performed in this report were for the European XFEL undulator lines SASE1, a fixed-gap device, and SASE2, which has a variable gap. The influence of reduced overlap in both insertion devices has been studied for random quadrupole offsets and for systematic undulator entrance and exit kicks. The wavelengths studied are the minimum wavelength of 0.1 nm and 0.4 nm, where the long wavelength can be achieved by reducing the energy (SASE1 and SASE2) or by decreasing the undulator gap (SASE2 only). From the simulation results presented we conclude the following.

1. Quadrupole offset simulation for several operation modes for SASE1 and SASE2 have been investigated. For each mode the FODO period is respectively set as 12 m and 24 m. The simulation result shows that when FODO period is 24 m, the RMS beam wander is smaller than when FODO period is 12 m, and power degradation is smaller.
2. Two kinds of undulator end-kick are simulated, one is that the kick direction is same at undulator entrance and exit, the other is that the kick direction is opposite. The opposite direction kick permits about ten times larger kick than the same direction end-kick.
3. Both of quadrupole offset and undulator end-kick can induce beam wander  $\sigma_r$ , as well as phase shake  $\sigma_\phi$ . More study on the parametric dependence between power reduction and a combination of these two parameters is needed.
4. Second order effects, such as the influence of undulator focusing and the wavelength shift due to an increased transverse velocity component, can be neglected for the parameter range studied here.

## Appendix A: Wavelength change due to a $y$ -dependent undulator field for off-axis electron beams

The transverse movement can introduce phase shake by two ways, one is that transverse momentum reduces the longitudinal velocity so that the ponderomotive phase will vary as well. Another one is that beam wander in  $y$ -direction changes the undulator field, which shifts the resonant wavelength. In this section we compare the phase shake due to these two effects.

First we talk about radiation wavelength variation by electron longitudinal velocity reduction. The longitudinal speed including transverse movement is:

$$\beta_z = \sqrt{1 - \frac{1}{\gamma^2} - \beta_\perp^2} \approx 1 - \frac{1 + a_u^2}{2\gamma^2} - \frac{\beta_\perp^2}{2} \quad (3)$$

we express the  $\beta_\perp$  as

$$\beta_\perp \approx \frac{\beta_\perp}{\beta_z} \equiv \theta, \quad (4)$$

where  $\theta$  denotes the angle between electron velocity to the axis. The resonance condition should satisfy:

$$\beta_z(\lambda_u + \lambda_s) = \lambda_u \quad (5)$$

Induce Eq.(3) and Eq. (4) the wavelength is:

$$\lambda_s = \frac{\lambda_u(1 + a_u^2)}{2\gamma^2} + \frac{\lambda_u}{2}\theta^2 \quad (6)$$

The first part in the right hand in Eq. (6) is the 1D FEL resonance condition. So second term holds the radiation wavelength variation because of transverse movement, we rewrite it as:

$$\Delta\lambda_{s,1} = \frac{\lambda_u}{2}\theta^2 \quad (7)$$

Then we talk about radiation wavelength variation by  $a_u$  changing because of  $y$ -direction offset. For a planer undulator, the undulator parameter  $a_u$  depends on the position on  $y$ -direction:

$$a_u = \frac{eB_0}{\sqrt{2}mck_u} \left( 1 + \frac{y^2 k_u^2}{2} \right), \quad (8)$$

where  $y$  denotes to the electron deviates from axis in  $y$  direction. The radiation wavelength variation because of  $a_u$  change can be described as:

$$\frac{\Delta\lambda_{s,2}}{\lambda_s} = \frac{2a_u\Delta a_u}{1 + a_u^2} = \frac{k_u^2 a_u^2}{1 + a_u^2} y^2 \quad (9)$$

In FODO structure, sinus function is good for describing electron trajectory. So the transverse movement can be described as:

$$y(z) = Y \sin(k_\beta z) \quad (10)$$

Where  $k_\beta$  and  $Y$  are respectively the period and amplitude of beta oscillation. So  $\theta$  is:

$$\theta = \frac{dy}{dz} = Yk_{\beta} \cos(k_{\beta}z). \quad (11)$$

Then we know the wavelength variation ratio by the two factors is:

$$\frac{\Delta\lambda_{s,1,rms}}{\Delta\lambda_{s,2,rms}} = \frac{\lambda_u^2 \gamma^2}{a_u^2 \lambda_{\beta}^2} \gg 1. \quad (12)$$

This means the phase shake generated by  $a_u$  variation because of y-direction offset can be neglected.

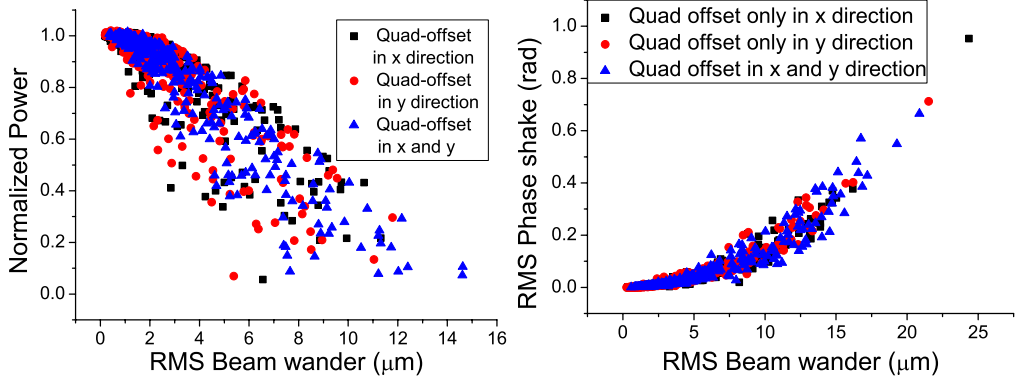


Figure 18: *Illustration of radiation power and RMS phase shake variation as RMS beam wander. Three kinds of quadrupole offset have been simulated: Quad offset only on x direction, Quad offset only on y direction and both on x and y direction. SASE1, 0.1 nm parameters are used here. Left: Normalized power degradation as different RMS beam wander; Right: RMS phase shake variation as RMS beam wander.*

Fig. 18 shows the power and RMS phase shake variation as RMS beam wander changes. The quadrupole offset is divided into offset in x-direction, offset in y-direction and in both x and y direction. It can be seen that the simulation result is similar to each other. Due to only the offset in y direction induce error to  $a_u$ , the similar result numerically means the  $a_u$  error by beam wander in y direction can be neglected. In this plot SASE1, 0.1 nm parameters are used as the example to do the simulation.

Due to no apparent difference among setting quadrupole offset in x or y direction or in both x and y direction, therefore we include quad-offset in both x and y direction.

## Appendix B: Wavelength shift due to phase shake

As discussed in the previous appendix, the wavelength variation generated by longitudinal velocity spread is much larger than the variation due to changes in the undulator parameter  $a_u$ . So in this section we discuss only the wavelength variation by longitudinal velocity variation.

The impact of a variation in transverse movement on the radiation wavelength can be investigated in the frame of ponderomotive phase shake. In an ideal undulator system electrons will always be synchronized with optic field so that the phase shake will be zero. If transverse movement exists, phase variation is

$$\phi' = k_u - k_s \frac{1 + a_u^2 + p_x^2 + p_y^2}{2\gamma^2} = -k_s \frac{p_x^2 + p_y^2}{2\gamma^2}, \quad (13)$$

where the resonant term has been subtracted. The wavelength variation can be calculated from the remaining angle ( $d\phi/dz$ ), as shown in Fig. 3.

$$\frac{\Delta\lambda_s}{\lambda_s} = \frac{\lambda_u}{2\pi} \frac{d\phi}{dz}. \quad (14)$$

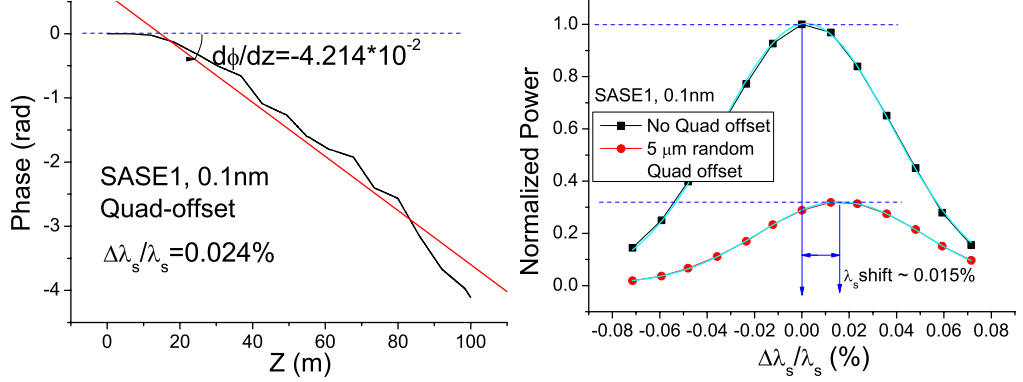


Figure 19: Wavelength scan for quad-offset. Left: Illustration of ponderomotive phase variation, the wavelength shift can be analytically calculated out from it; Right: simulation result of wavelength scan. The power is normalized by the number without error. The chosen point is 70% saturation length.

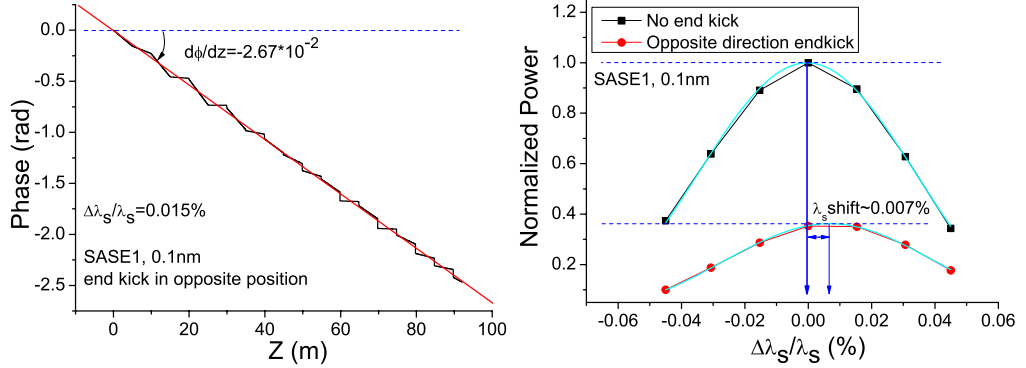


Figure 20: Wavelength scan for undulator end-kick, the kick direction is opposite. Left: Illustration of ponderomotive phase variation, the wavelength shift can be analytically calculated out from it; Right: simulation result of wavelength scan. The power is normalized by the number without error. The chosen point is 70% saturation length.

To illustrate the wavelength shift, we do several simulation for quadrupole offset and undulator end-kick. Fig. 19, Fig. 20 and Fig. 21 illustrate the simulation result. The left plots in these figures shows the wavelength shift analytically calculated out from Eq. 21. The right plot shows the numerical simulation. We can see that the optimized

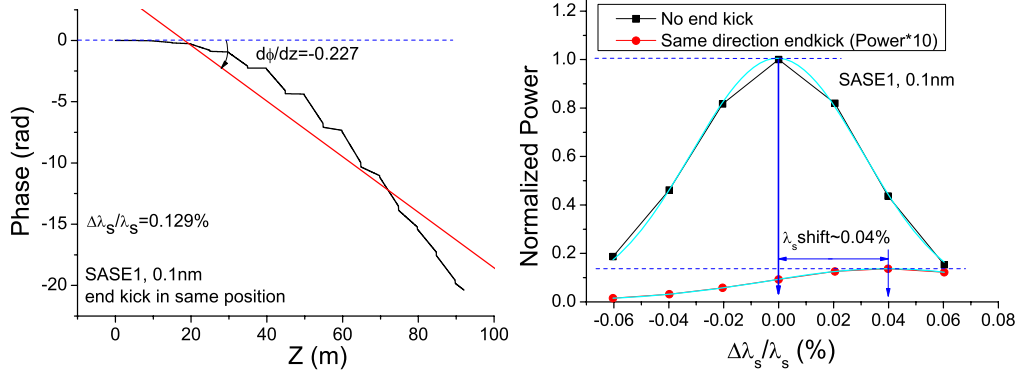


Figure 21: Wavelength scan for undulator end-kick, the kick direction is same. Left: Illustration of pondermotive phase variation, the wavelength shift can be analytically calculated out from it; Right: simulation result of wavelength scan. The power is normalized by the number without error. The chosen point is 70% saturation length.

wavelength really changes when the error is included while the shift amount is smaller than the number analytically evaluated. While actually it can be seen that the shift is very small so that this difference is understandable.

Because hundreds of random simulation is required for the Quad offset simulation, so it is very difficult to scan the wavelength for all of the simulations. Due to the very small optimized wavelength shift, therefore for the quadrupole simulation in this report, we fix the wavelength to the optimized value without quadrupole offset. On the other hand for the end-kick simulation, due to only tens of simulations are required, so for each simulation we scan the wavelength and pick the optimized value as the result.

## Appendix C: Modification of RMS beam wander

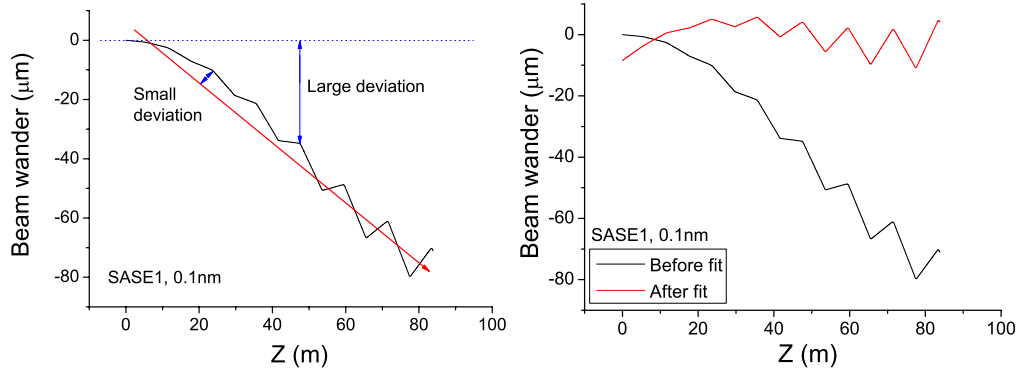


Figure 22: Beam orbit caused by undulator end-kick. Left: beam deviation compared to a straight orbit. Right: beam wander before and after subtraction of a linear fit.

In this section we discuss the calculation of RMS beam wander. As illustrated in previous section,  $\sigma_r$  can be calculated in a normal way:

$$\sigma_r = \sqrt{\frac{1}{l} \int_0^l (r(z) - \bar{r})^2 dz}, \quad (15)$$

where  $r$  is the deviation from the axis. Fig. 22 shows the beam orbit caused by an undulator end-kick. One can see that the electron beam center largely deviates from the undulator axis. So if the RMS beam wander is calculated by Eq. (15) the beam wander will be relatively large and the expected power degradation will be large too. While the fact is, as the beam mainly moves on one direction (red arrow) deviating from the undulator axis, so the radiation power will also concentrate on this direction. Therefore it is more reasonable taking the red arrow line instead of undulator axis as the base to determine the value of  $r$ .

To do this first we calculate the beam orbit and linearly fit it with function  $y = a \cdot z + b$ , and then calculate out the modified orbit deviation  $r'$ :

$$r'(z) = r(z) - (az + b) \quad (16)$$

$$\sigma_r = \sqrt{\frac{1}{l} \int_0^l (r'(z) - \bar{r}')^2 dz}$$

where  $a$  and  $b$  are coefficients of the fitted line.

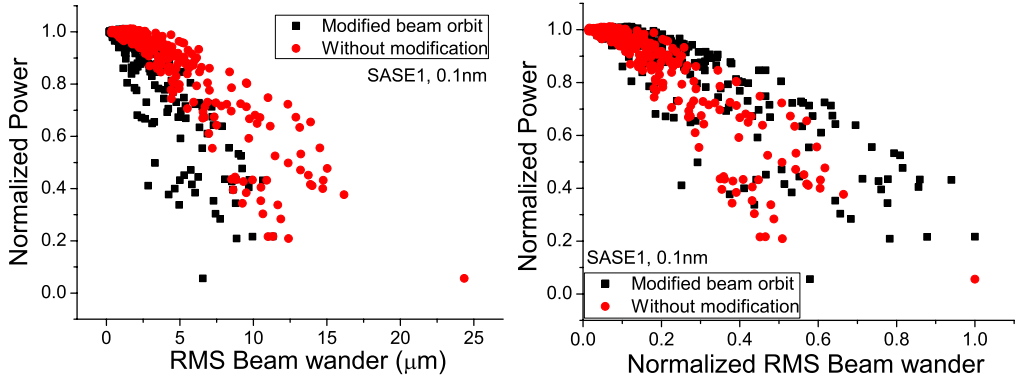


Figure 23: *Power degradation by beam wander. The beam wander is calculated by two methods, one is from the beam deviation from undulator axis, another is deviation from a fitted line. In this figure, only x-direction Quad offset is induced. Left: beam wander unit is chosen  $\mu\text{m}$ ; Right: Beam wander is normalized by their respective largest beam wander value.*

Fig. 23 shows the power degradation by beam wander, which is calculated with or without modifying beam orbit. The parameter of SASE1, 0.1 nm is utilized here. From the left plot, one can see that after modifying the beam orbit, the beam wander is smaller than before.

Moreover, due to the modification changes the RMS beam wander, so in the left plot it is difficult to see how the impact by the modification to power spread at a certain RMS beam wander value. Therefore in the right plot the RMS beam wander is normalized by their respective largest beam wander value. From it one can see that the power spread is similar at a same value.

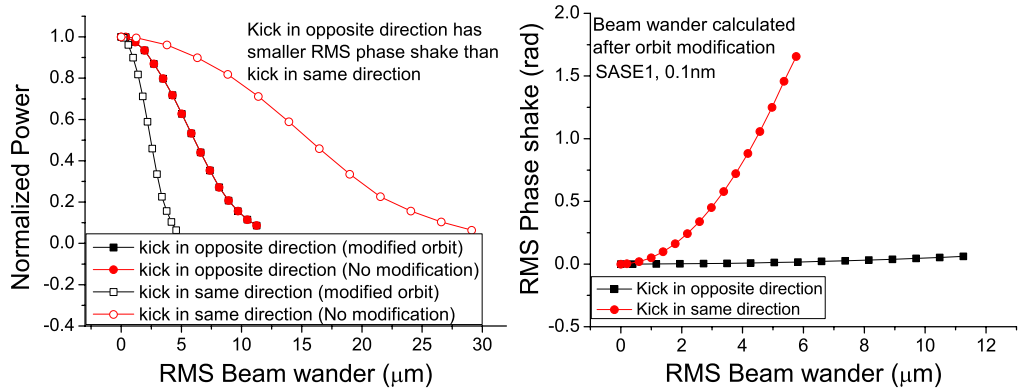


Figure 24: *Left: Power degradation by beam waver for undulator end-kick simulation. Right: RMS phase shake variation at different RMS beam waver. Kicking on opposite direction has smaller RMS phase shake. From this figure, straightening beam orbit gives reasonable result.*

Fig. 23 shows for the quadrupole offset. Then Fig. 24 shows the orbit modification impact to undulator end-kick. It can be seen that for the opposite direction end-kick, the RMS beam waver does not change much if modifying or not the orbit. While for the same direction end-kick, the RMS beam waver changes greatly: if the beam orbit is modified, at a same RMS beam waver kicking in opposite direction degrades smaller power than kicking on same direction. If the beam orbit is not modified, at a same RMS beam waver kicking in opposite direction degrades larger power than kicking on same direction.

Combine the RMS phase shake we can do some compare. As analyzed in last section, both beam waver and phase shake reduct radiation power. From the right plot in Fig. 24, at a same RMS beam waver value, kicking in opposite direction gives smaller RMS phase shake, so if the orbit is not modified, the result can not be understood: why same RMS beam waver and smaller RMS phase shake degrades larger radiation power? Therefore, for the end-kick simulation, modifying beam orbit gives reasonable result.

Therefore, for all of the result, the RMS beam waver is calculated after modifying the beam orbit.

## Appendix D: The relation between beam waver and RMS phase shake

Electron transverse momentum can induce beam waver and thus reduce the overlap between electron and optical field such that it degrades the FEL performance. In addition, as mentioned in the section before, transverse movement can induce phase shake which also reduces the FEL performance. Since both beam waver and phase shake are induced by transverse movement, we briefly discuss the relation between them. The ponderomotive phase change is:

$$\phi' = k_u - k_s \frac{1 + a_u^2 + p_x^2 + p_y^2}{2\gamma^2}. \quad (17)$$

In this report the undulator parameter  $a_u$  always refers to the ideal value, so that the

resonance condition reads:

$$k_u - k_s \frac{1 + a_u^2}{2\gamma^2} = 0. \quad (18)$$

Therefore, the phase change can be written as

$$\phi' = -k_s \frac{p_x^2 + p_y^2}{2\gamma^2}. \quad (19)$$

The transverse speed is:

$$x' = \frac{p_x}{\gamma}, y' = \frac{p_y}{\gamma}. \quad (20)$$

Since the phase depends on the square of the transverse momentum and the position depends on this linearly, as first approximation one can assume that power reduction depends on a combination of the rms phase shake and on the square of the beam wander. Fig. 25 shows the numerical result for SASE1 for 0.1 nm. We can see that the numerical calculation also shows that the RMS phase shake  $\sigma_\phi$  is proportional to the square value of RMS beam wander  $\sigma_r$ .

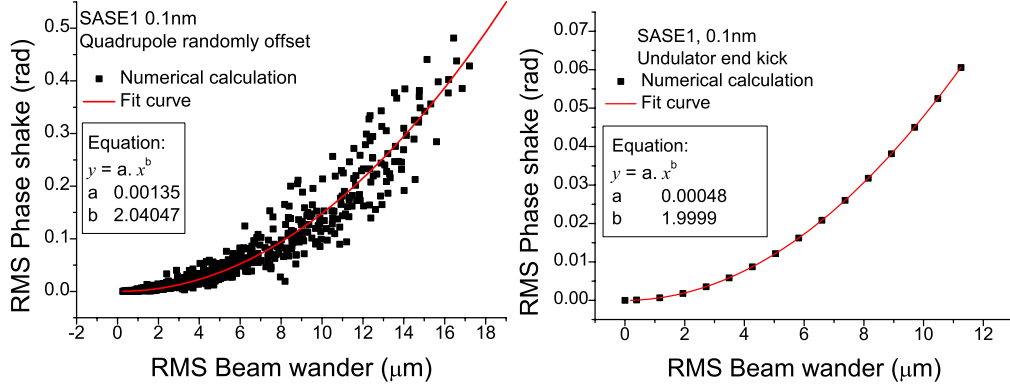


Figure 25: Relationship between RMS phase shake and RMS beam wander caused by random quadrupole offset (left) and due to undulator end-kick (right).

## References

- [1] Massimo Altarelli et.al., The European X-Ray Free-Electron Laser Technical Design Report, ISBN 3-935702-17-5
- [2] A.M. Kondratenko and E.L. Saldin, Part. Accel. 10, 207 (1980)
- [3] R. Bonifacio, C. Pellegrini, and L.M. Narducci, Opt. Commun. 50, 373 (1984)
- [4] J. Pflueger, *Undulator Systems and Photon Diagnostics for the European XFEL Project*, Proceedings of the 27th International Free Electron Laser Conference (2005) 378-382
- [5] B.L. Bobbs et.al, Nucl. Instr. and Meth. **A296** (1990) 574-578
- [6] B. Faatz, J. Pflueger, Y.M. Nikitina, Nucl. Instr. and Meth. **A393** (1997) 380-384

- [7] J. Pflueger, M. Tischer, Nucl. Instr. and Meth. **A483** (1999) 388-393
- [8] Y. Li, B. Faatz and J. Pflueger, Study of Undulator Tolerances for the European XFEL, TESLA-FEL report 2007-07, DESY, Hamburg.
- [9] S. Reiche, Nucl. Instr. and Meth. **A429** (1999) 243-248